Biophysical Reports

ARTICLE

Fibrin prestress due to platelet aggregation and contraction increases clot stiffness

Suyog J. Pathare,[1] Wilson Eng,[2] Sang-Joon J. Lee,[2,*] and Anand K. Ramasubramanian[1,*]
[1]Department of Chemical and Materials Engineering and [2]Department of Mechanical Engineering, San José State University, San José, California

ABSTRACT Efficient hemorrhagic control is attained through the formation of strong and stable blood clots at the site of injury. Although it is known that platelet-driven contraction can dramatically influence clot stiffness, the underlying mechanisms by which platelets assist fibrin in resisting external loads are not understood. In this study, we delineate the contribution of platelet-fibrin interactions to clot tensile mechanics using a combination of new mechanical measurements, image analysis, and structural mechanics simulation. Based on uniaxial tensile test data using custom-made microtensometer and fluorescence microscopy of platelet aggregation and platelet-fibrin interactions, we show that integrin-mediated platelet aggregation and actomyosin-driven platelet contraction synergistically increase the elastic modulus of the clots. We demonstrate that the mechanical and geometric response of an active contraction model of platelet aggregates compacting vicinal fibrin is consistent with the experimental data. The model suggests that platelet contraction induces prestress in fibrin fibers and increases the effective stiffness in both cross-linked and noncross-linked clots. Our results provide evidence for fibrin compaction at discrete nodes as a major determinant of mechanical response to applied loads.

WHY IT MATTERS Strength of blood clots is determined by the remodeling of fibrin by the contractile forces exercised by the platelets in the later stages of clotting. Therefore, determining how platelet-fibrin interactions increase clot stiffness is fundamental to the understanding of hemostasis and thrombosis. Here, we show from uniaxial tensile strain and quantitative microscopy data that the elastic moduli of blood clots correlate directly to the ability of platelets to aggregate and to apply prestress to fibrin fibers. A quasistatic contraction model based on the experimental data explains that the contractile fibrin-bound platelet aggregates act as prestressed nodes and increase the effective stiffness of the entire clot.

INTRODUCTION

Efficient hemostasis culminates in the formation of strong and stable plugs to dam blood flow in broken vessels or to stop leaks through injured vessel walls. The strength and stability of clots are important predictors of bleeding diathesis and thrombotic complications, and these properties are being adopted for new indications including trauma and anticoagulant monitoring (1,2). Clot components including platelets, fibrinogen, and red blood cells (RBCs) contribute to the mechanical properties of the clot (3–6). The dynamics of interactions between these components on clot mechanics is an active area of investigation because of fundamental importance and translational benefits.

Fibrin is the key structural element of a clot. Platelets not only initiate and propagate fibrin formation but also modify the structure of the fibrin network extensively during the later stages of clotting through retraction. The hemostatic potential of the platelets, including their ability to activate, to aggregate, and–most importantly–to retract, determines the clot stiffness (7–9). It was recently shown that clot contraction and enhanced clot stiffness are the results of exquisitely organized, platelet-driven, and actomyosin- and integrin-mediated remodeling of fibrin (10). However, the mechanism by which platelet contraction enhances resistance of a clot against applied forces is unknown, and this question is of fundamental importance to the understanding of hemostasis.

To answer this question, first, we evaluate the stress-strain behavior of blood clots to uniaxial tensile strain

Submitted August 20, 2021, and accepted for publication September 8, 2021.

*Correspondence: sang-joon.lee@sjsu.edu or anand.ramasubramanian@sjsu.edu

Editor: Kandice Tanner.

https://doi.org/10.1016/j.bpr.2021.100022

using a custom-made microtensometer. To our knowledge, this is the first study to report the elastic properties of fresh human blood clots subjected to tensile strain. Uniaxial testing is a direct method to measure the tensile mechanical properties of several (vascular) biomaterials, including fibrin gels (11), collagen gels (12), stored porcine blood clots (13), cell-seeded scaffolds (14), and aortic tissue (15). Together with appropriate mathematical models, tensile tests have provided profound insights into the mechanobiology of cell-matrix interactions (16–19). Second, using the experimental tensile and microstructural data in conjunction with a computational model for the response of fibrin to platelet compaction strain and externally applied strain, we elucidate the relationship between platelet-fibrin interactions and the mechanical response of clots to applied extension. We discover that platelet aggregates compacted with dense fibrin bundles act as prestressed nodes that dramatically increase the stiffness of the entire clot.

MATERIALS AND METHODS

Measurement of clot response to uniaxial strain

Blood was obtained from healthy adult human volunteers in 3.2% sodium citrate, and clotting was initiated within 15 min of blood draw after recalcification with final concentration of 20 mM $CaCl_2$ (Sigma-Aldrich, St. Louis, MO) (20). The clotting process was initiated by the addition of final concentration of 1 U/mL thrombin to 500 μL of recalcified blood, and the clot was incubated under humidified conditions for 1.5 h for full contraction (21). The clots were gently separated from the serum and loaded onto the clamps of a custom-made microtensometer. The microtensometer consists of a motorized nanopositioner (MP-285; Sutter Instrument, Novato, CA), a full-bridge thin cantilever load cell (113 g, LCL Series; OMEGA Engineering, Norwalk, CT), and a data acquisition signal conditioner DI-1000U (Loadstar Sensors, Fremont, CA). The load cell was zeroed without the bottom support to neglect the weight of the clot in the initial pull. The force recording from the data acquisition software (LoadVUE; Loadstar Sensors) and actuation of the nanopositioner were started simultaneously, and force measurements were recorded at 30 Hz. Two digital cameras were positioned at orthogonal angles to capture top-view and side-view images to extract the cross-sectional dimensions. Cross-section images were used to convert force-displacement curves to the respective true stress versus stretch ratio curves.

In designated cases, the following inhibitors were added to blood and incubated for 30 min at room temperature with gentle rocking (Vari-Mix Platform Rocker; Thermo Fisher Scientific, Waltham, MA) at $\sim$2 Hz before recalcification: 300 μM blebbistatin, 10 μM eptifibatide, or 10 μM T101. To investigate the effect of platelets in clotting, RBCs were separated by centrifugation for 15 min without brakes at 250 relative centrifugal force, 7 rad/s^2 acceleration, and after separating the RBCs from platelet-rich plasma, platelet-poor plasma (PPP) was obtained by further centrifugation of platelet-rich plasma for 20 min without brakes at 1500 relative centrifugal force, 7 rad/s^2 acceleration. The RBC was added back to PPP to restore the hematocrit to original levels in the whole blood. The hematocrit levels were estimated based on compacted RBC volume after centrifugation, and it typically ranged between 40 and 50%.

Microstructural characterization of clots

To visualize clot microstructure, platelets and fibrinogen were labeled with Alexa Fluor 488 (AF488) and Alexa Fluor 596 (AF596) fluorophores, and 100 μL of blood was used to form clots as described above. Platelets in whole blood were incubated with an AF488-conjugated CD42b antibody for 20 min before the start of clotting, and blood was doped with 5% AF596-conjugated fibrinogen, assuming a final concentration of 4 mg/mL. After 1.5 h, the clots were imaged at 63$\times$ magnification using an oil immersion lens (DMi8; Leica Microsystems, Wetzlar, Germany). Z-stack images were collected from at least five different locations for each clot. The fluorescence images were processed and analyze offline for quantification by two-dimensional (2-D) projection of the stack to estimate aggregate size and Pearson correlation coefficient (PCC) using Image-Pro 10 (Media Cybernetics, Rockville, MD) and ImageJ (National Institutes of Health).

Discrete prestressed fiber model simulations

Simulations were based on structural mechanics for a finite number of 2-D truss elements, with the platelet aggregate located within a prescribed initial radius R_0 at the center of a square region. Equal displacement and force equilibrium are maintained at the node, joining each "within aggregate" and "outside of aggregate" fiber. Given symmetry about two planes, only the upper right quadrant was necessary for simulations. Material properties were assigned distinctly to the line segments inside and outside of the prescribed radius. Poisson's ratio was kept constant at a value of 0.49, assuming nearly ideal incompressibility. The elastic modulus of the interior line segments was based on relative modulus-β, defined as the ratio of elastic modulus of compacted fibrin to noncompacted fibrin. The effect of compaction was simulated by prescribing a compaction strain-α, defined as the extent of reduction from an initial radius R_0 to a compacted radius R_c (i.e., $\alpha = (R_0 - R_c)/R_0$). The compaction strain provides a prestress that is analogous to the stress that would result from the strain associated with thermal shrinkage. Thus, the variable material inputs are fibrin Young's modulus, relative modulus (for platelets), and compaction strain.

Simulations were performed using COMSOL Multiphysics (Stockholm, Sweden), using quasistatic 2-D truss elements with geometric nonlinearity enabled such that the direction of tension remained axial as each element changed orientation throughout the prescribed extension. Strain energy densities were simulated using parametric sweeps along values of compaction strain-α and applied uniaxial strain-ε, up to a strain of 50%. Compaction strain-α was mimicked using a thermal expansion coefficient. Convergence of the discrete fiber model was checked by varying the number of fibers and evaluating the average strain energy density. The range of solution values among five-fiber, six-fiber, and seven-fiber solutions was less than 0.6% of the mean (Fig. S3 *A*), and five fibers were used for all reported strain energy density simulations. For all clots involving platelets (i.e., untreated, blebbistatin, eptifibatide, and T101), geometric dimensions were set to match the compacted radius that was determined from image analysis. The relative size of the model quadrant was customized according to the spatial density of aggregates, which was determined by computing the average number of aggregates per unit area for each type of clot. The corresponding lengths of fibrin fibers were set to maintain the relative size of a single platelet aggregate to ensure correct proportion of aggregate area with respect to the bounding-box quadrant of the fiber model. The corresponding relative sizes (i.e., aggregate radius divided by quadrant box edge length) for untreated, blebbistatin-treated, eptifibatide-treated, and T101-treated clots were 0.087, 0.100, 0.103, and 0.118, respectively. Thus, the geometric model inputs are the number of fibers, bounding-box size, and initial aggregate radius.

Statistical analysis

The data were collected from clots prepared from five to seven different donors, and the experiments were performed on different days. For each donor and treatment, the microtensometry experiments were performed at least in triplicate, and the results from two or three replicates for each donor were averaged. To establish differences between untreated and treated clots, a paired, one-tailed Student's *t*-test was performed to calculate *p*-values, for which a value of less than 0.05 was deemed statistically significant.

RESULTS

Mechanical characterization of blood clots

Response of blood clots to uniaxial strain

To measure the stress-strain response of blood clots in the ranges of micronewton force and submicron displacement, we designed a microtensometer that measures tension as the clots are stretched (Fig. 1 *A*). The design specifications, engineering details, and calibration of the instrument are presented elsewhere (22). Thrombin-initiated whole blood clots were loaded onto the microtensometer and secured using magnetic clamps (Fig. 1 *A*; Fig. S1). Clots having a 6-mm gauge length were extended by 3 mm (i.e., 50% strain) at 100 μm/s. Force measurements were recorded simultaneously at 30 Hz. The force-displacement curves were converted to true stress versus strain plots using cross-sectional area measured in two orthogonal directions (23). As expected for many biological tissues and fibrous-matrix materials, the stress-strain plot for untreated whole blood clots exhibits strain-stiffening behavior over the tested range of strains (Fig. 1 *B*). Next, we evaluated the contribution of platelets to the mechanical behavior of clots using blood reconstituted with PPP and obtained the stress-strain response as outlined above (Fig. 1 *B*). The clots from reconstituted blood without platelets were substantially more compliant than whole blood clots. The strain energy density, which is the potential energy stored in the clot due to the work done to deform the clot, is computed as the area under the stress-strain curve. At 50% strain, the strain energy density of whole blood clots was nearly twofold higher than that of clots formed without platelets, suggesting that the platelets contribute nearly twofold more work in deforming the clots (Fig. 1 *C*). The equivalent linear stiffness of the clot at 50% strain, which is the slope of an ideally linear stress-strain curve having the same strain energy density, was estimated to be 4.4 kPa, which is in the same range of Young's modulus values reported recently for retracted clots using micropillars (9). The equivalent linear stiffness of clots without platelets was substantially lower at 2.5 kPa.

To parameterize the stress-strain response, we applied an empirical nonlinear fit using a uniaxial simplification of the Fung strain energy model that has been widely used for soft tissues composed of fibrous networks (24). For this model, the strain energy is given by $u = C_0 \exp(a_1\varepsilon^2)$, where u is the strain energy density, ε is uniaxial strain, and C_0 and a_1 are fitted constants. Differentiating strain energy with respect to strain, we obtain an expression for tensile stress as $\sigma = 2C_0\, a_1\, \varepsilon \exp(a_1\, \varepsilon^2)$. The stress-strain experimental data were fitted to this equation (Fig. 1 *D*). The variables C_0 and a_1 parameterize stiffness at lower strains and strain-stiffening behavior, respectively. The estimates for C_0 and a_1 for whole blood clots are, as expected, significantly lower than those reported for aortic tissues (25,26) (Fig. 1 *E*). In the absence of platelets, the stress-strain curve fits yielded estimates of C_0 and a_1 that are threefold lower and twofold higher, respectively, than untreated clots. Because the stress-strain relationship is nonlinear, the elastic modulus of the clot increases with tensile strain and can be estimated from the equivalent area under the stress-strain curve. As can be seen from Fig. S2 *A*, platelets contribute to a nearly twofold increase in stiffness of the clots over the entire range of strain tested in this work.

Effect of platelet contraction and aggregation on clot response to uniaxial strain

Having established the role of platelets to the stress-strain response of blood clots, we sought to determine the role of two key processes, i.e., platelet compaction and aggregation, which are known to impact the overall contraction of a blood clot. To this end, we evaluated the stress-strain response of clots formed with platelets treated with blebbistatin, in which clot formation was initiated by the addition of thrombin. Blebbistatin inhibits the binding of myosin II to actin, which is critical to platelet contraction (27). As shown in Fig. 1 *C*, we observed that blebbistatin treatment significantly changed the response of clots to uniaxial strain compared with untreated clots. From these plots, we computed the total strain energy density, the nonlinear fit parameters, and the stiffness at 50% strain. The strain energy density was 25% lower in clots treated with blebbistatin compared with untreated clots (Fig. 1 *C*).

To evaluate the effect of platelet aggregation on the tensile response of the clots, we similarly tested clots prepared using platelets exposed to eptifibatide, an inhibitor of platelet GP IIb/IIIa, and hence aggregation (28). The uniaxial stress response shows that these clots are weaker than untreated clots, although only modestly so (Fig. 1 *C*). The strain energy density for eptifibatide-treated clots was 20% lower than for that of untreated clots (Fig. 1 *C*). The parameter C_0 was lower for blebbistatin- and eptifibatide-treated clots,

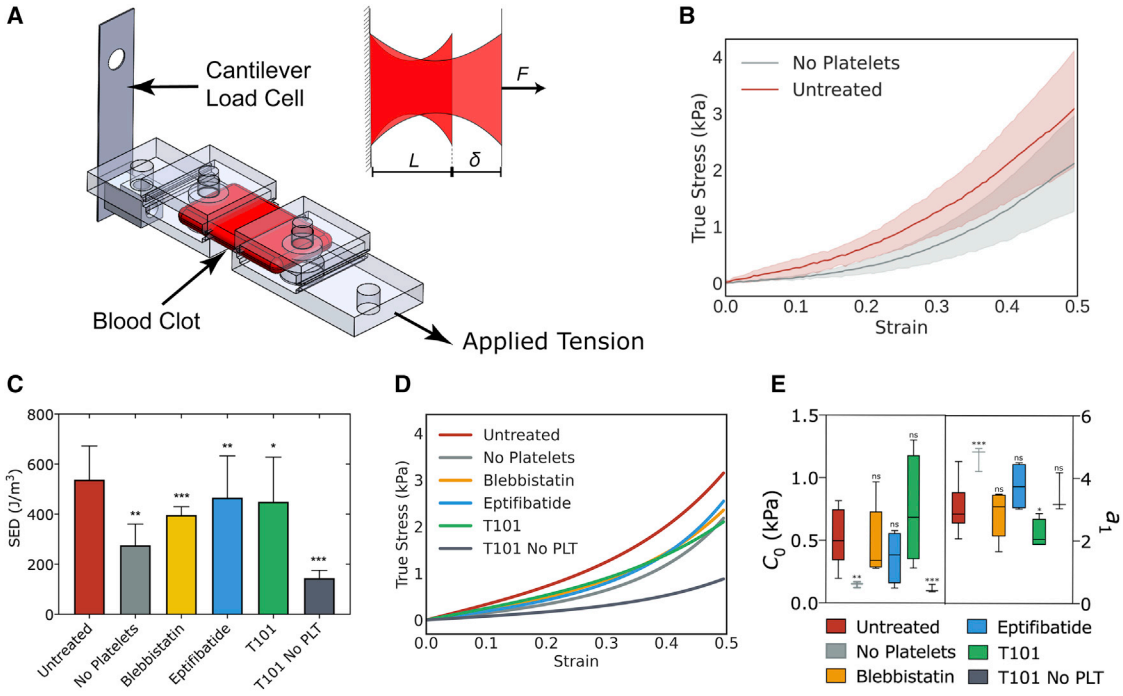

FIGURE 1 Response of blood clots to uniaxial strain. (*A*) Oblique view and close-up top view of clot in between microtensometer grips. One grip is attached to a fixed load cell, and the opposite of the grip is moved by a nanopositioner.(*B*) Stress-strain response of clots formed by the addition of thrombin to whole blood or clots formed from platelet poor plasma reconstituted with RBCs. (*C*) Strain energy densities at 50% strain. (*D*) Stress-strain curves fitted to the nonlinear exponential model $\sigma = 2C_0a_1\exp(a_1\varepsilon^2)$, where σ is stress, ε is strain, and C_0 and a_1 are model parameters. (*E*) C_0 and a_1 for untreated and treated clots. Mean $\pm$ standard deviation, $*p < 0.05$, $**p < 0.01$, $***p < 0.001$.

indicative of overall lower stiffness. The parameter a_1 was only modestly different from that of whole blood clots, indicative of similar strain-stiffening behavior (Fig. 1 *E*; Fig. S2 *A*). To evaluate how much platelet aggregation and contraction contributes to the stiffness of whole blood clots over that only due to fibrin cross-linking, we normalized the increase in strain energy density of eptifibatide- and blebbistatin-treated clots over platelet-poor (i.e., "no-platelet") clots by the increase in strain energy density of platelet-rich whole blood clots over platelet-poor clots. This calculation shows that eptifibatide and blebbistatin treatments reduce clot stiffness by 51 and 67%, respectively.

Of note, the tensile modulus of the no-platelet clots in the 1-kPa range is comparable with the previous measurements of tensile modulus of fibrin gels in the 2–10-kPa range (29). It is instructive to place the tensile elastic modulus *E* estimated in this work with other well-known measures of clot stiffness: shear modulus, *G*′, estimated by rheometry, and the maximal amplitude estimated by thromboelastography. It has been shown that maximal amplitude and *G*′ are significantly impacted by the inhibitors of GP IIb/IIIa or actin polymerization, similar to the microtensometry results. However, a direct comparison between these measurements and our results is limited not only because the of differences in types of strain (shear strain versus tensile strain) applied to the sample but also because in rheometry and thromboelastography, clots contain serum, whereas in tensometry, the contracted clots do not contain serum (20,30).

Contribution of fibrin cross-linking on clot response to uniaxial strain

To evaluate the effect of fibrin cross-linking, we evaluated the stress response of clots that were polymerized with thrombin but in the presence of T101. T101 inhibits transglutaminase activity of FXIII, thereby eliminating the lateral cross-linking of fibrin strands (20,31). The strain energy density of noncross-linked clots was ~25% lower than that of cross-linked clots. We observed that noncross-linked clots show significantly lower stress at the same strain, i.e., weaker, compared with the clots formed by the direct addition of thrombin (Fig. 1 *D*). Correspondingly, the stiffness of 2.1 kPa at 50% strain was comparable with clots without platelets, indicating that the platelets are as influential as cross-linking in clots initiated with exogenous thrombin. The C_0-value was comparable with untreated whole blood clots, but a_1 was lower, revealing the relative importance of cross-links on stiffness at higher strains and that this is evident from weaker dependence of elastic modulus with applied strain (Fig. S2 *B*). The combined effect of cross-linking and platelets

on clot stiffness can be seen from T101-treated blood without platelets. These clots were the weakest with strain energy density threefold lower than that of whole blood clots (Fig. 1 *C*).

Microstructural characterization of platelet-fibrin interactions in clots

As seen from the mechanical data, platelets contribute to the stiffness of the clots through platelet contraction and aggregation. To understand the contribution of platelets, we analyzed clot microstructure through high-magnification fluorescence imaging, with emphasis on platelet-fibrin interactions in clots prepared from platelets that were untreated or treated with blebbistatin or eptifibatide (Fig. 2 *A*). As evidenced by the intensity of red and green fluorescence due to fibrin and platelets, respectively, interfering with platelet actomyosin or aggregation altered the size of the aggregates and the amount of fibrin present. Interestingly, T101 treatment did not seem to alter either platelet aggregates or the amount of fibrin present on the platelets.

To quantify platelet-fibrin interactions, we first estimated the size of platelet aggregates and the amount of fibrin in these aggregates. The average sizes computed based on these images revealed a mean aggregate size of 40 μm^2 in clots without any treatment, whereas blebbistatin and eptifibatide treatments reduced the average aggregate size by twofold and threefold, respectively (Fig. 2 *B*). In contrast, T101 treatment only had a modest effect on aggregate size. Next, we correlated the spatial distributions of the densities of platelets and fibrin based on the overlap in the fluorescence intensities between platelets (green, CD42b-AF488) and fibrin (red, fibrinogen-AF596) using the PCC (Fig. 2 *C*). A PCC closer to 1.0 signifies a higher incidence of localization between the green and red fluorophores (32). We observed that in untreated blood clots, 80% of the projected area of the platelet aggregates was also fibrin rich. In contrast, the spatial overlap between fibrin and platelet densities was low in clots formed from blebbistatin-treated platelets. PCC was only modestly affected by eptifibatide-treated clots, indicating that single platelets or microaggregates co-located strongly with fibrin. A similarly small difference in PCC compared with untreated clots was observed in clots treated with T101, suggesting that fibrin cross-linking may only modestly affect the colocalization of fibrin fibers on platelet aggregates.

Both platelet aggregation and fibrin compaction determine clot stiffness

Upon observing the effect of platelet aggregation and platelet actomyosin on clot stiffness from microtensometry and also the effect on platelet-fibrin interactions from microstructure studies, we sought to establish a relationship between the two. We estimated the equivalent modulus based on strain energy density at 50% strain. We surmised that the size of the platelet aggregates and the amount of the fibrin bound to platelet aggregates, i.e., PCC, would be critical to clot stiffness. Although neither the size nor PCC individually show a meaningful correlation with equivalent modulus, we discovered that the product of these quantities, which estimates the density of the fibrin bound to platelet aggregates, is tightly correlated with the equivalent modulus of the clot (Fig. 3). The effect

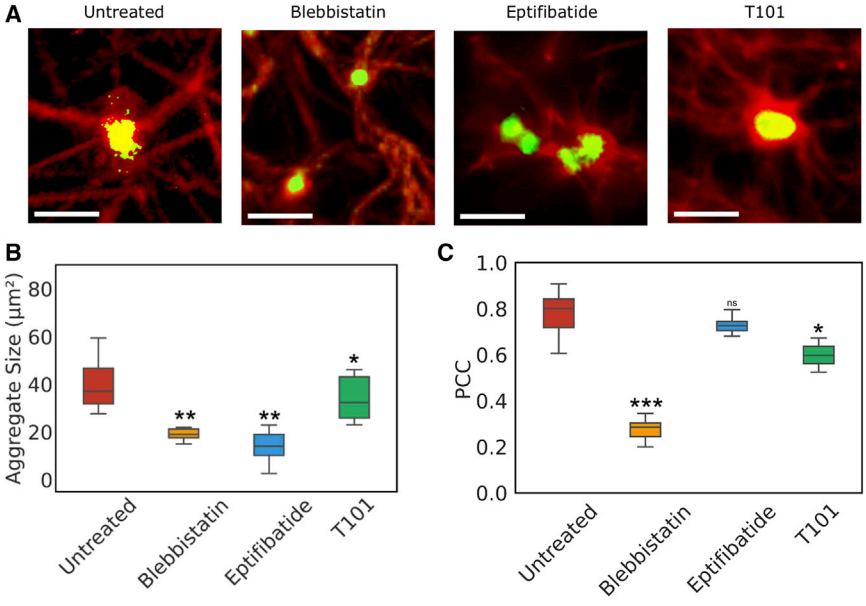

FIGURE 2 Microstructural characterization of platelet-fibrin aggregates. (*A*) Clots prepared from platelets that were either untreated or treated with blebbistatin, eptifibatide, or T101. Scale bars, 10 μm; Platelets are labeled with AF488-CD42b (*green*) and fibrinogen with AF594-fibrinogen (*red*). (*B*) Average size of platelet aggregates. (*C*) PCC for the colocalization of platelets and fibrin. Mean ± standard deviation, *$p < 0.05$; **$p < 0.01$; ***$p < 0.001$.

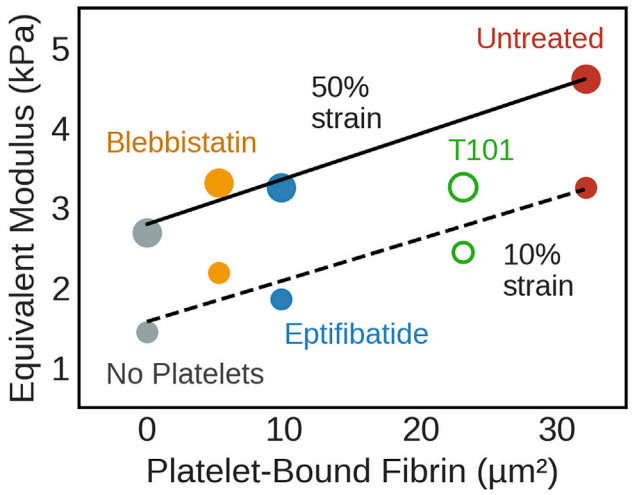

FIGURE 3 Platelet-fibrin interactions determine clot stiffness. Elastic modulus correlates linearly with the density of platelet-bound fibrin at various applied strains. The lines represent least-square best fits without T101 (with $R^2 = 0.90$ at 10% strain and $R^2 = 0.97$ at 50% strain, respectively).

of the fibrin bound to the platelet aggregates on elastic modulus was independent of applied strain (i.e., slope of 52–57 kPa/μm^2 over 10–50% strain), indicating that the fibrin-platelet interactions determine the effective mechanical behavior of the clot. These data show that both platelet aggregation and actomyosin contraction result in comparable densities of fibrin-bound platelet aggregates, and they contribute similarly to increasing the stiffness beyond the baseline no-platelet clot, albeit by different mechanisms. Interestingly, disrupting fibrin cross-linking with T101 had two effects: it not only reduced the amount of fibrin bound to the platelet aggregates but also lowered the equivalent modulus from what may be expected of fully cross-linked clots.

A computational framework for understanding the contribution of fibrin-bound platelet aggregates on clot stiffness

The passive fiber adsorption model

Having established a correlation between the density of fibrin-bound platelet aggregates and strain energy density, we sought to develop a computational model to interrogate the underlying physical basis of this relationship. We posited that the fibrin adsorbed on platelet aggregates will result in an increase in the elastic modulus of platelet-fibrin aggregates over that of the fibrin matrix in the bulk. The platelet-fibrin aggregate is represented by a contractile element with an elastic modulus E_c, which may be different from the modulus of elastic modulus E_f of distal fibers (Fig. 4 *A*). The ratio between moduli is defined as relative modulus, $\beta = E_c/E_f$. The fibers are bound to platelet GP IIb/IIIa receptor clusters at the focal adhesion sites located at a radial distance R_c.

Effect of fiber modulus on the strain energy density of the clots

Finite element simulations were performed using truss-element fibers at evenly spaced angles in a quadrant with two-plane symmetry (Fig. 4 *B*). The node (shared by all fibers) at the origin was fixed, and nodes on the right-side boundary were assigned prescribed uniaxial displacements, as indicated in Fig. 4 *B*. The two nodes along the top side are assigned correspondingly proportional strains according to their horizontal positions (i.e., mimicking a roller condition for a continuous body). The model showed convergence in strain energy density with as few as three fibers per quadrant, and simulations presented here used five fibers per quadrant (Fig. S3 *A*). Fig. 4 *C* shows the distribution of local deformation of the fibrin fibers under the combined effect of platelet contractile strain and externally applied strain. As expected, the fibers oriented in the direction of externally applied strain experienced the largest magnitudes of local displacement. However, we notice that merely passive spring elements failed to capture experimental observations. In the absence of compaction strain, even a 10-fold increase in elastic modulus of the fibrin bound to the platelet aggregates produced a barely perceptible increase in strain energy density (Fig. 4 *D*).

The discrete prestressed fiber model

Next, we modified the above model to replace passive platelet-fibrin spring elements with actively contracting platelet-fibrin aggregates. A discrete prestressed fiber model and its functional components that include a fibrin-bound platelet aggregate are shown in Fig. 5 *A*. Similar to the previous model, the platelet-fibrin aggregate is represented by a contractile element with an elastic modulus E_c, which may be different from the modulus of elastic modulus E_f of distal fibers, and the ratio between moduli is defined as relative modulus, $\beta = E_c/E_f$. To account for platelet contraction, the fibers are bound to platelet GP IIb/IIIa receptor clusters at the focal adhesion sites located at a radial distance R_0 from the center of the aggregate. Contractile forces during clotting due to actomyosin activity draw fibers inward, and these fibers are retracted to a tighter aggregate of radius R_c. This contraction induces a prestressed condition in the vicinity of the aggregate, and the prestress is retained by the clot even in the absence of an externally applied load. A quasistatic model of platelet contraction is a realistic approximation because the timescale of contraction-relaxation of nonmuscle myosin IIA is much smaller than the timescale of matrix contraction (33). This prestress is due to

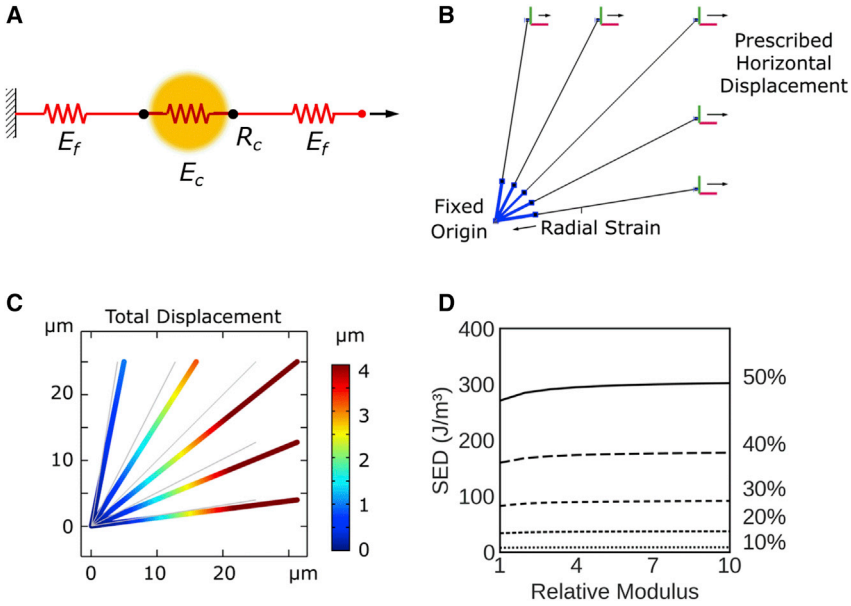

FIGURE 4 Passive fiber adsorption model. (*A*) Fibrin fibers (*red*) are connected to fibrin-bound platelets (*yellow*), and both fibers are modeled as springs with different stiffnesses. In this passive model, platelets do not exercise any active contractile stress. (*B*) Description of model elements and boundary conditions. (*C*) Representative deformation of a five-fiber model with a 5-μm aggregate radius and relative modulus of 10, pulled to 25% uniaxial strain. (*D*) Strain energy density as a function of relative modulus at various applied strains up to 50%.

plasticity of the overall cell-matrix interaction, as has been observed for cells encapsulated in collagen and fibrin gels (34). Fig. 5 *B*, superimposed on the average stress-strain curve of the clots without platelets (i.e., fibrin network), illustrates how prestress can influence the effective modulus. In the absence of prestress, an externally applied strain ε_{ext} results in a nominal stress σ_{nom}. The local modulus at the corresponding nominal strain ε_{nom} is E_{nom}. However, when prestress σ_{pre} and prestrain ε_{pre} are present, the addition of the same externally applied strain results in a higher effective stress σ_{eff}, and the local effective modulus E_{eff} at the (total) effective strain ε_{eff} is steeper. The corresponding strain energy density, computed as the area under the curve up to the effective strain, is also substantially larger than nominal.

The interaction between a representative fibrin fiber bundle and a platelet aggregate is depicted in Fig. 5 *C*. Platelet GP IIb/IIIa-fibrin(ogen) interactions anchor the fibrin fibers to the platelet surface. The fiber of an initial length L_0 is bound to the platelet aggregate at a focal adhesion at point *O*. A quarter circle that represents a single platelet aggregate with two orthogonal planes of symmetry is shown within a corresponding quadrant of a square having side length *b*. The fiber is oriented at an arbitrary angle θ with respect to the direction of applied external strain. The fiber *OP* experiences the combined effects of prestrain and applied external strain, resulting in a geometrically nonlinear response to strain. The individual fibers are modeled as linear elastic materials obeying Hooke's law.

The global stiffness matrix for two fibers in series is written as shown in Eq. 1, where node 0 is at the center of a platelet aggregate, node 1 is at the focal adhesion, and node 2 is the free end subject to external strain. *F* represents nodal forces and *d* represents nodal displacements along the axial direction *x*. Spring constants k_1 and k_2 are associated with the platelet aggregate and (unbound) fibrin fiber, respectively.

$$\begin{Bmatrix} F_{0x} \\ F_{1x} \\ F_{2x} \end{Bmatrix} = \begin{bmatrix} k_1 & -k_1 & 0 \\ -k_1 & k_1+k_2 & -k_2 \\ 0 & -k_2 & k_2 \end{bmatrix} \begin{Bmatrix} d_{0x} \\ d_{1x} \\ d_{2x} \end{Bmatrix}. \quad (1)$$

To represent prestress, we add a contractile force $F = -\alpha EA$ and the focal adhesion (i.e., node 1), where the elastic modulus *E* and cross-sectional area *A* pertain to the platelet aggregate. The parameter α is the compaction strain, defined as the extent of aggregate compaction from an initial radius R_0 to a compacted radius R_c (i.e., $\alpha = (R_0 - R_C)/R_0$). At node 2 (i.e., the location where external strain is applied), the fiber is subjected to a horizontal displacement δ. Applying these assigned conditions, the equilibrium solution to axial force along the fiber assembly is as shown in Eq. 2, with details provided in the Supporting materials and methods.

$$F = \left(k_2 - \frac{k_2^2}{k_1+k_2}\right)\delta + \frac{k_2 EA}{k_1+k_2}\alpha. \quad (2)$$

In the presence of prestrain due to compaction ($\alpha > 0$), the second term in the force solution above predicts a higher axial force along the fiber with increasing compaction strain. From this solution, the corresponding strain energy density can be calculated for any combination of relative modulus-β, compaction strain-α, and

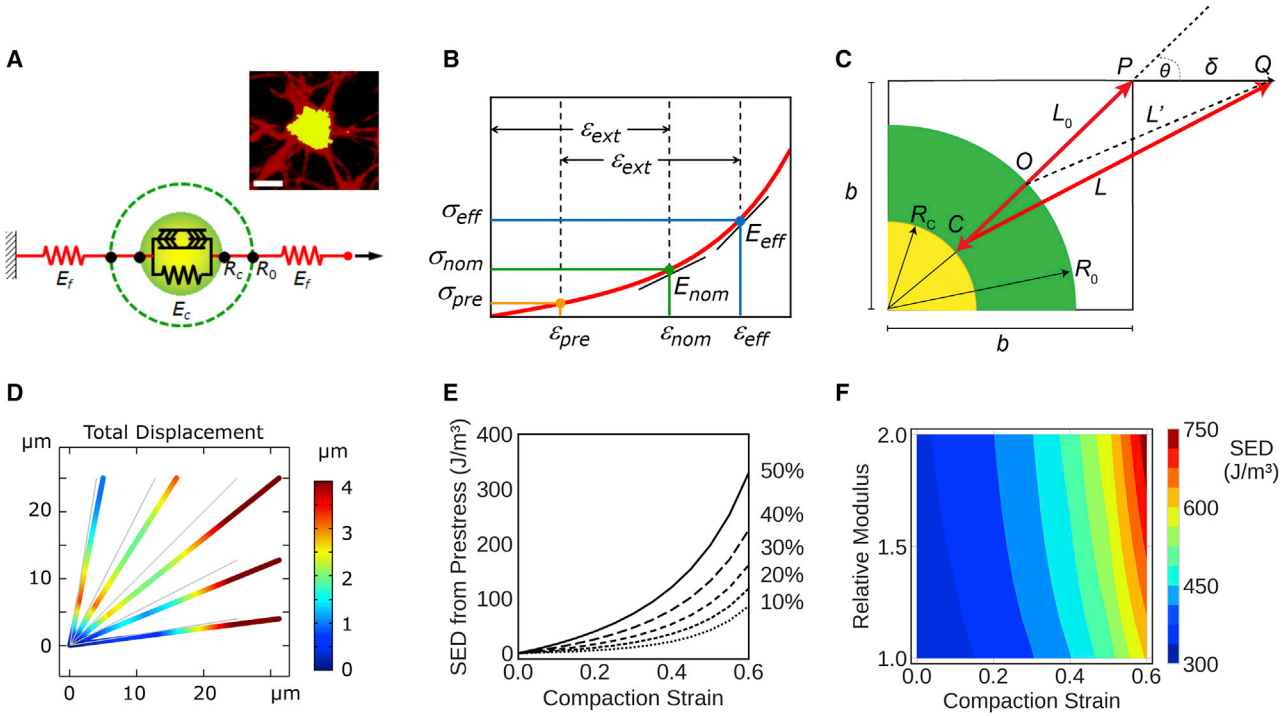

FIGURE 5 Discrete prestressed fiber model for clot subjected to uniaxial strain. (*A*) The actomyosin contractile elements in platelets compact the fibrin fibers onto the aggregates. Given is the representative image of a single platelet aggregate with fibers emanating from the aggregate (scale bars, 5 μm) (*inset*). (*B*) Compaction strain is added to externally applied strain such that the effective modulus E_{eff} is higher than nominal; (*C*) Euclidean geometric representation of a fibrin fiber compacted by platelet contraction. (*D*) Representative finite element simulation of fiber deformation in the vicinity of a platelet aggregate, shown with a 5-μm aggregate radius, 0.5 compaction ratio, 2.0 relative modulus, and 25% applied strain. (*E*) Strain energy density due to prestress as a function of compaction strain for applied strain up to 50%. (*F*) Predicted strain energy density as a function of compaction strain and relative modulus.

applied uniaxial strain $\varepsilon = \delta/b$. The multidirectional orientation of fibers was accounted for by using coordinate transformations for fibers that are oriented off axis from the direction of externally applied strain, as explained in the Supporting materials and methods.

Effect of fibrin compaction and fiber modulus on the strain energy density of the clots

Fig. 5 *D* shows the results of finite element simulations on the distribution of local deformation of the fibrin fibers under the combined effect of platelet contractile strain and externally applied strain. As expected, the fibers oriented in the direction of externally applied strain experienced the largest magnitudes of local displacement. For the same applied strain, the absence of platelets resulted in smaller local deformation of the fibers when compared with the deformation in the presence of platelet contraction (Fig. 5 *D* vs. Fig. S3 *B*). In the absence of platelets, the strain energy density of the fibrin fibers is purely due to externally applied strain and scales approximately as the square of strain (Fig. S3 *C*).

We computed strain energy densities using the five-element model for a range of compaction strains and externally applied strains. The compacted radius R_c and the bounding-box size b for each clot type were set accordingly to account for the average space occupied by a single platelet aggregate, based on the average density of aggregates measured from image analysis. Because strain energy density is additive, the effect of applied strain can be subtracted from the total strain energy density to obtain the effect of compaction strain. As shown in Fig. 5 *E*, we observed that the contribution to strain energy density from compaction increases exponentially with an increase in compaction strain and is more pronounced at higher externally applied strains because the fibers are effectively subjected to strains in a steeper region of the stress-strain curve.

The above simulations were performed assuming that the elastic modulus of the fibrin fibers is twice as much upon compaction on the platelet surface as when they are not bound to platelets. Because the actomyosin stress fibers are indeed rigidity sensors and respond to the increase in local stiffness by exerting larger traction forces, we also considered the effect of an increase in the elastic modulus of fibrin fibers that get compacted on the platelet surface due to contraction (35) (Fig. 5 *F*). We noticed that the total strain energy density was only modestly affected by

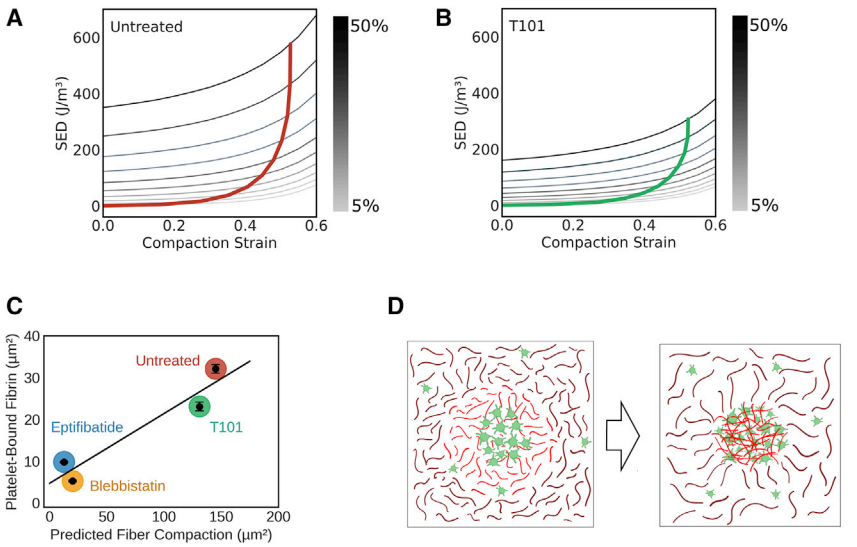

FIGURE 6 Discrete prestressed fiber model predicts the amount of fibrin fiber compacted by contracting platelets. (*A* and *B*) Mapping of experimentally determined strain energy density onto model predictions for cross-linked (*A*) and uncross-linked clots (*B*). The sets of grayscale lines plot simulated SED as a function of radial compaction strain (*horizontal axis*) for increasing values of externally applied tensile strain (*grayscale bar*). The single colored lines (*red* for untreated and *green* for T101) show the loci of intersections with experimentally measured SED at each level of applied strain. (*C*) Correlation between experimentally determined fibrin density on platelet surface and predicted fiber compaction based on area reduction ($R^2 = 0.91$). (*D*) Schematic representation of predicted fiber compaction by platelets. Platelet aggregates sequester fibrin fibers into dense nodes, thereby prestressing the fibers close to platelets.

the platelet-bound fibrin as being stiffer than unbound fibrin over a broad range of compaction strains. From these simulations, we demonstrated that our discrete fiber model accounts for the effects of both compaction strain due to platelets and strain due to externally applied tension, in agreement with the total strain energy density measured experimentally.

Fibrin compaction on platelet surface due to aggregation and actomyosin contraction increases the strain energy density of clots

Next, we sought to obtain estimates of compaction strain by matching the total strain energy density from model predictions against experimentally measured values. Because the simulations show that the relative modulus has only a modest effect on strain energy density over the experimental range (i.e., 300–750 J/m^3), without loss of generality, we considered a model wherein the modulus of the fiber increased by twofold upon compaction (Fig. 5 *E*). To compare the model predictions with experimental stress-strain data, we superimposed the experimentally determined strain energy densities at different applied strains (computed from Fig. 2 *A*) on to the model predictions (Fig. 6, *A* and *B*). To establish a baseline case without platelets (Fig. S2 *B*), the model with only fibrin fibers (i.e., $R_0 = 0$) was first calibrated to the average stress-strain curve of no-platelet clots to match the Young's modulus that was consistent with strain energy density at each 10% increment of external uniaxial strain between 10 and 50%. The corresponding Young's modulus values varied between 3.5 and 4.7 kPa over this range of strain. To establish a second baseline, a case with no fibrin cross-linking (and no platelets) was established based on average stress-strain data of clots treated with T101. The corresponding Young's modulus values for the weaker fibers (i.e., without the benefit of cross-linking) varied between 1.8 and 2.1 kPa. Because the applied tensile strain increases beyond ∼20% and the resistance to deformation is due to fibrin fibers bound to platelets, the intersections between experimental and predicted strain energy densities converge at a characteristic compaction strain of ∼0.6.

Similarly, we estimated the compaction strain for clots formed from platelets treated with blebbistatin or eptifibatide (Fig. S4, *A* and *B*). Both blebbistatin and eptifibatide treatments significantly reduced the compaction strain to nearly threefold lower than for untreated platelets, indicating that both platelet aggregation and actomyosin contraction are critical in increasing the effective modulus of the clot. As shown in Fig. 6 *B*, for clots treated with T101, the predicted compaction strain was comparable with that of untreated clots, indicating that disrupting cross-linking of fibrin fibers does not alter the ability of the platelets to contract the fibrin fibers. For computing the compaction strain in T101-treated clots, we used the elastic modulus of fibrin fibers estimated from clots formed from blood depleted of platelets and also treated with T101. The elastic modulus of these clots formed from blood depleted of platelets but treated with T101 were much lower than the elastic modulus of clots treated with T101, indicating the significant impact of fibrin cross-linking on clot properties.

Fibrin compaction predicted from the model correlates with proportion of fibrin on platelet aggregates

As discussed above, the compaction strain predicted by the discrete fiber model provides a measure of fibrin

densification on the platelet surface. In Fig. 6 *C*, we observe that this is indeed the case, as the total amount of fibrin sequestered onto the platelet surface due to compaction strain is linearly correlated to the fibrin bound to platelet aggregates, as estimated by the product of PCC and aggregate area. This observation suggests that the extent of colocalization on aggregates observed by microscopy may serve as an effective quantitative metric for estimating fibrin compaction that leads to prestress in the clots. We note that the amount of fibrin compacted by platelets decreases by fivefold if the actomyosin contraction or aggregation is inhibited, as evident from blebbistatin or eptifibatide treatments, respectively. Interestingly, the amount of fibrin compacted by platelets was not as strongly influenced by the ability of fibrin to cross-link, suggesting that the decrease in elastic modulus of T101-treated clots is caused mainly by lack of cross-linking in the matrix rather than by the inability of fibrin to interact with platelet aggregates.

DISCUSSION

Both conventional rheometry and more recent micropost measurements have shown that the presence of platelets increases the stiffness of clots by, depending on the measurement techniques, twofold to fivefold in the 0.8–20-kPa range (9,20,36). The increase in clot stiffness is a result of clot retraction, volume shrinkage, and plasma exudation driven by platelet contraction. As platelets contract, they appear to tug along the fibrin fibers and actively remodel fibrin in their vicinity (10,37). However, the biophysical mechanisms by which these platelet-fibrin interactions increase clot stiffness is unknown. We show that the work done by contracting platelets in remodeling the fibrin fibers is stored as strain energy density even before an external load is applied and is a critical contribution to the mechanism by which the clots resist deformation (38). Analogous to macroscopically familiar structures such as a rope hammock or an anchor capstan, our experimental data and modeling support the hypothesis that the discrete prestressed nodes composed of fibrin-bound platelet aggregates are key to the structural stability of the clots (39) (Fig. 6 *D*).

The local contractile strain exerted by platelets on vicinal fibrin is somewhat similar to that from the contractile strain exercised on the extracellular matrix by contracting cells which remodels fibers in the immediate vicinity of the cells and increases the overall stiffness of fibrous-matrix gels (40,41). However, there are several important distinctions between the contractile strain exerted by platelets vis-à-vis fibroblasts: first, although cells rearrange the fibrous networks of the extracellular matrix in their immediate vicinity, platelet filopodia draw and spool the fibrin fibers inward so much that the platelets are wrapped in fibrin fibers, as evidenced by the colocalization indices. We have deliberately used the term "compaction strain" instead of "contractile strain" to underscore this distinction. Second, compared with cellular traction forces, the contractile forces generated by single platelets are more than an order of magnitude lower in the 2–20-nN range, suggesting that platelet aggregation may be key to compensating for the smaller size and force (42–44) compared with fibroblasts. Our experimental data suggest that this is indeed the case: 1) although disrupting platelet aggregation using eptifibatide did not alter platelet-fibrin interactions (i.e., PCC) at the single platelet level, it significantly weakened the clot; and 2) based on the increase in the stiffness of whole blood clots (4.4 kPa) compared with no-platelet clots (2.5 kPa), and using an average platelet aggregate diameter of 7 μm, we can estimate the mean contractile force exerted by a platelet aggregate to be in the few hundreds of nanonewtons, which is in a range comparable with cellular traction forces (45). Third, simultaneous and cooperative compaction of fibrin by platelet aggregates is likely to be important in increasing clot stiffness because neither activated, but poorly aggregating platelets nor a-priori-aggregated platelets retract efficiently (46,47). Our computational results confirm that this is indeed the case because only the model accounting for active platelet contraction but not passive stiffening of platelet-fibrin aggregates is capable of matching experimental strain energy density measurements.

A prominent result from this study is that fibrin that is taken in by the contraction of platelet aggregates from their immediate vicinity is sufficient to increase resistance to deformation substantially for the entire clot, even though most of the matrix may remain agnostic to platelet contraction. As a corollary, if the platelet-fibrin aggregates were not prestressed, to provide the strain energy density equivalent to that of a whole blood clot, the entire fibrin gel would have to be twice as stiff. This increase in stiffness would have to arise purely from higher levels of fibrin polymerization and cross-linking. In light of growing interest and relevance on the spatial heterogeneity in the composition of in vivo clots to their strength (48,49), our results, to our knowledge, present some of the first insights into the origins of clot response to external forces. We expect that these insights will lead to more detailed expositions of clot deformation through the use of appropriate image-based three-dimensional models of the network, accounting for nonlinear fiber properties, viscoelastic characteristics of the clot as well as the modification of these properties by red cell concentration, and deformability by platelet concentration and by platelet-fibrin interactions.

In summary, we have measured the elastic moduli of blood clots subjected to uniaxial tensile strain using microtensometry, and we have estimated the contribution of platelet contraction and aggregation to clot stiffness using specific inhibitors of nonmuscle myosin IIA, aggregation, and cross-linking. Our results show that the platelet contribution to clot stiffness is dominated by nodes in the fibrous matrix that are composed of platelet aggregates and compacted fibrin. The concept of nodal prestress introduced in this work provides insights into how fibrin sequestering during clot retraction serves as a key stabilizing factor in clot mechanics. The experimental and computational framework presented in this work, for the first time, to our knowledge, not only measures tensile properties of clots but also provides a simple yet powerful model to establish mechanobiological relationships between intracellular stress and tissue-scale external loads.

SUPPORTING MATERIAL

Supporting material can be found online at https://doi.org/10.1016/j.bpr.2021.100022.

AUTHOR CONTRIBUTIONS

S.J.P. and W.E. performed experiments and analyzed the data. S.-J.L. performed the computational studies. S.-J.L. and A.K.R. conceived the research, designed the experiments, performed the data analysis, procured funding, and wrote the manuscript. All authors approved the manuscript.

DECLARATION OF INTERESTS

The authors declare no competing interests.

ACKNOWLEDGMENTS

Assistance with data collection from C. Puligundla, L. A. Resnikowski, J. Alzaghari, and S.-M. Saw is gratefully acknowledged.

This work was supported by funds from the American Heart Association (18AIREA33960524), the National Science Foundation (Award #1727072), and the California State University Program for Education and Research in Biotechnology.

REFERENCES

1. Spahn, D. R., B. Bouillon, …, R. Rossaint. 2019. The European guideline on management of major bleeding and coagulopathy following trauma: fifth edition. *Crit. Care.* 23:98.
2. Hartmann, J., M. Murphy, and J. D. Dias. 2020. Viscoelastic hemostatic assays: moving from the laboratory to the site of care-a review of established and emerging technologies. *Diagnostics (Basel).* 10:118.
3. Jen, C. J., and L. V. McIntire. 1982. The structural properties and contractile force of a clot. *Cell Motil.* 2:445–455.
4. Ryan, E. A., L. F. Mockros, …, L. Lorand. 1999. Structural origins of fibrin clot rheology. *Biophys. J.* 77:2813–2826.
5. Chueh, J. Y., A. K. Wakhloo, …, M. J. Gounis. 2011. Mechanical characterization of thromboemboli in acute ischemic stroke and laboratory embolus analogs. *AJNR Am. J. Neuroradiol.* 32:1237–1244.
6. Tutwiler, V., R. I. Litvinov, …, J. W. Weisel. 2016. Kinetics and mechanics of clot contraction are governed by the molecular and cellular composition of the blood. *Blood.* 127:149–159.
7. Reid, T. J., R. Snider, …, B. M. Alving. 1998. A method for the quantitative assessment of platelet-induced clot retraction and clot strength in fresh and stored platelets. *Vox Sang.* 75:270–277.
8. Ting, L. H., S. Feghhi, …, N. J. Sniadecki. 2019. Contractile forces in platelet aggregates under microfluidic shear gradients reflect platelet inhibition and bleeding risk. *Nat. Commun.* 10:1204.
9. Chen, Z., J. Lu, …, R. Zhao. 2019. Microclot array elastometry for integrated measurement of thrombus formation and clot biomechanics under fluid shear. *Nat. Commun.* 10:2051.
10. Kim, O. V., R. I. Litvinov, …, J. W. Weisel. 2017. Quantitative structural mechanobiology of platelet-driven blood clot contraction. *Nat. Commun.* 8:1274.
11. Lai, V. K., S. P. Lake, …, V. H. Barocas. 2012. Mechanical behavior of collagen-fibrin co-gels reflects transition from series to parallel interactions with increasing collagen content. *J. Biomech. Eng.* 134:011004.
12. Susilo, M. E., J. A. Paten, …, J. W. Ruberti. 2016. Collagen network strengthening following cyclic tensile loading. *Interface Focus.* 6:20150088.
13. Krasokha, N., W. Theisen, …, H. Monstadt. 2010. Mechanical properties of blood clots - a new test method. *Materialwiss. Werkstofftech.* 41:1019–1024.
14. Upton, M. L., C. L. Gilchrist, …, L. A. Setton. 2008. Transfer of macroscale tissue strain to microscale cell regions in the deformed meniscus. *Biophys. J.* 95:2116–2124.
15. Keyes, J. T., D. G. Haskett, …, J. P. Vande Geest. 2011. Adaptation of a planar microbiaxial optomechanical device for the tubular biaxial microstructural and macroscopic characterization of small vascular tissues. *J. Biomech. Eng.* 133:075001.
16. Wang, H., A. S. Abhilash, …, V. B. Shenoy. 2014. Long-range force transmission in fibrous matrices enabled by tension-driven alignment of fibers. *Biophys. J.* 107:2592–2603.
17. Ban, E., H. Wang, …, V. B. Shenoy. 2019. Strong triaxial coupling and anomalous Poisson effect in collagen networks. *Proc. Natl. Acad. Sci. USA.* 116:6790–6799.
18. Charras, G., and A. S. Yap. 2018. Tensile forces and mechanotransduction at cell-cell junctions. *Curr. Biol.* 28:R445–R457.
19. Markert, C. D., X. Guo, …, M. Guthold. 2013. Characterizing the micro-scale elastic modulus of hydrogels for use in regenerative medicine. *J. Mech. Behav. Biomed. Mater.* 27:115–127.
20. Nair, P. M., S. G. Pandya, …, A. K. Ramasubramanian. 2017. Platelets stored at 4°C contribute to superior clot properties compared to current standard-of-care through fibrin-crosslinking. *Br. J. Haematol.* 178:119–129.
21. Tutwiler, V., H. Wang, …, V. B. Shenoy. 2017. Interplay of platelet contractility and elasticity of fibrin/erythrocytes in blood clot retraction. *Biophys. J.* 112:714–723.
22. Eng, W., M. Kim, …, S.-J. J. Lee. 2018. A modular test platform for micromechanical tensile testing of soft biomaterials. In Proceedings of the ASME 2018 International Mechanical Engineering Congress and Exposition. Volume 3, Biomedical and Biotechnology Engineering. American Society of Mechanical Engineers https://asmedigitalcollection.asme.org/IMECE/proceedings/IMECE2018/52026/273663.
23. Eng, W. S. 2018. Nonlinear stiffness and viscoelasticity of inhibitor-treated blood clots by tensile testing. Master's thesis. San

Jose State University https://scholarworks.sjsu.edu/etd_theses/4964.

24. Fung, Y. C. 1980. On pseudo-elasticity of living tissues. *In* Mechanics Today. S. N. Nasser, ed. Pergamon Press Ltd, pp. 49–66. https://doi.org/10.1016/B978–0-08–024249–1.50014–5.
25. Holzapfel, G. A. 2006. Determination of material models for arterial walls from uniaxial extension tests and histological structure. *J. Theor. Biol.* 238:290–302.
26. Niestrawska, J. A., C. Viertler, …, G. A. Holzapfel. 2016. Microstructure and mechanics of healthy and aneurysmatic abdominal aortas: experimental analysis and modelling. *J. R. Soc. Interface.* 13:20160620.
27. Limouze, J., A. F. Straight, …, J. R. Sellers. 2004. Specificity of blebbistatin, an inhibitor of myosin II. *J. Muscle Res. Cell Motil.* 25:337–341.
28. O'Shea, J. C., and J. E. Tcheng. 2002. Eptifibatide: a potent inhibitor of the platelet receptor integrin glycoprotein IIb/IIIa. *Expert Opin. Pharmacother.* 3:1199–1210.
29. Williams, C., E. Budina, …, L. D. Black, III. 2015. Cardiac extracellular matrix-fibrin hybrid scaffolds with tunable properties for cardiovascular tissue engineering. *Acta Biomater.* 14:84–95.
30. Lang, T., W. Toller, …, G. Halwachs-Baumann. 2004. Different effects of abciximab and cytochalasin D on clot strength in thrombelastography. *J. Thromb. Haemost.* 2:147–153.
31. Freund, K. F., K. P. Doshi, …, A. M. Stern. 1994. Transglutaminase inhibition by 2-[(2-oxopropyl)thio]imidazolium derivatives: mechanism of factor XIIIa inactivation. *Biochemistry.* 33:10109–10119.
32. Dunn, K. W., M. M. Kamocka, and J. H. McDonald. 2011. A practical guide to evaluating colocalization in biological microscopy. *Am. J. Physiol. Cell Physiol.* 300:C723–C742.
33. Gong, Z., S. E. Szczesny, …, V. B. Shenoy. 2018. Matching material and cellular timescales maximizes cell spreading on viscoelastic substrates. *Proc. Natl. Acad. Sci. USA.* 115:E2686–E2695.
34. Kim, J., J. Feng, …, B. Sun. 2017. Stress-induced plasticity of dynamic collagen networks. *Nat. Commun.* 8:842.
35. Trichet, L., J. Le Digabel, …, B. Ladoux. 2012. Evidence of a large-scale mechanosensing mechanism for cellular adaptation to substrate stiffness. *Proc. Natl. Acad. Sci. USA.* 109:6933–6938.
36. Carr, M. E., Jr., and S. L. Carr. 1995. Fibrin structure and concentration alter clot elastic modulus but do not alter platelet mediated force development. *Blood Coagul. Fibrinolysis.* 6:79–86.
37. Cohen, I., J. M. Gerrard, and J. G. White. 1982. Ultrastructure of clots during isometric contraction. *J. Cell Biol.* 93:775–787.
38. Wang, N., I. M. Tolić-Nørrelykke, …, D. Stamenović. 2002. Cell prestress. I. Stiffness and prestress are closely associated in adherent contractile cells. *Am. J. Physiol. Cell Physiol.* 282:C606–C616.
39. Lee, S.-J. J., D. M. Nguyen, …, A. K. Ramasubramanian. 2020. Image-based analysis and simulation of the effect of platelet storage temperature on clot mechanics under uniaxial strain. *Biomech. Model. Mechanobiol.* 19:173–187.
40. Reinhart-King, C. A., M. Dembo, and D. A. Hammer. 2008. Cell-cell mechanical communication through compliant substrates. *Biophys. J.* 95:6044–6051.
41. Hersch, N., B. Wolters, …, B. Hoffmann. 2013. The constant beat: cardiomyocytes adapt their forces by equal contraction upon environmental stiffening. *Biol. Open.* 2:351–361.
42. Lam, W. A., O. Chaudhuri, …, D. A. Fletcher. 2011. Mechanics and contraction dynamics of single platelets and implications for clot stiffening. *Nat. Mater.* 10:61–66.
43. Liang, X. M., S. J. Han, …, N. J. Sniadecki. 2010. Platelet retraction force measurements using flexible post force sensors. *Lab Chip.* 10:991–998.
44. Schwarz Henriques, S., R. Sandmann, …, S. Köster. 2012. Force field evolution during human blood platelet activation. *J. Cell Sci.* 125:3914–3920.
45. Maskarinec, S. A., C. Franck, …, G. Ravichandran. 2009. Quantifying cellular traction forces in three dimensions. *Proc. Natl. Acad. Sci. USA.* 106:22108–22113.
46. De Gaetano, G., M. B. Donati, …, M. Verstraete. 1971. Inhibition of clot retraction by previous in vitro platelet aggregation. *Thromb. Diath. Haemorrh.* 26:449–454.
47. Nair, P. M., H. F. Pidcoke, …, A. K. Ramasubramanian. 2014. Effect of cold storage on shear-induced platelet aggregation and clot strength. *J. Trauma Acute Care Surg.* 77 (*Suppl 2*):S88–S93.
48. Staessens, S., F. Denorme, …, S. F. De Meyer. 2020. Structural analysis of ischemic stroke thrombi: histological indications for therapy resistance. *Haematologica.* 105:498–507.
49. Chernysh, I. N., C. Nagaswami, …, J. W. Weisel. 2020. The distinctive structure and composition of arterial and venous thrombi and pulmonary emboli. *Sci. Rep.* 10:5112.

Biophysical Reports, Volume *1*

Supplemental information

Fibrin prestress due to platelet aggregation and contraction increases clot stiffness

Suyog J. Pathare, Wilson Eng, Sang-Joon J. Lee, and Anand K. Ramasubramanian

S1. Materials and Methods

Acquisition of human blood

Blood was obtained from donor volunteers according to the protocol approved by the Institutional Review Board (F16134) at San José State University. The donors were 18 to 25 years of age, healthy, free of any known bleeding or cardiovascular disorders, nondiabetic, and not under any platelet-function altering medication. The blood was drawn in 3.2% buffered sodium citrate vacutainer tubes (BD Biosciences, San Jose, USA).

Preparation of blood clots

500 µL of blood was recalcified by the addition of sterile-filtered $CaCl_2$ (Millipore Sigma, St. Louis, MO, USA) at pH 7.4 to a final concentration of 20 mM, and restriction grade thrombin (Millipore Sigma, St. Louis, MO, USA) to a final concentration of 0.2 U/mL in wells of a 25 mm x 75 mm chamber slide (Nunc, Rochester, USA) and allowed to clot for 90 min at room temperature. For designated experiments, the following inhibitors were added to blood, and incubated for 30 min at room temperature with gentle rocking (Vari-Mix Platform Rocker, Thermo Fisher Scientific, Waltham, MA, USA) at approximately 2 Hz before recalcification: blebbistatin (Calbiochem, San Diego, CA, USA) at 300 µM; eptifibatide (Bio-Techne Corp., Minneapolis, MN) at 10 µM; or T101 (Zedira GmbH, Germany) at 10 µM.

Measurement of clot response to uniaxial strain

Design and fabrication of custom microtensometer device

The microtensometer consists of a motorized nanopositioner (MP-285, Sutter Instrument, Novato, CA, USA), a full-bridge thin cantilever load cell (113 g, LCL Series, OMEGA Engineering, Norwalk, CT, USA), and a signal conditioner DI-1000U (Loadstar Sensors, Fremont, CA). The nanopositioner has a 25 mm range resolution of 40 nm per step. Speeds are selectable from 20 µm/s to 2.9 mm/s. The DI-1000U has 24-bit resolution and up to 80 Hz sampling rate.

An aluminum clamp with a recessed crevice that allowed for two points of contact was found to provide consistent clamping. A magnet was press-fit inside the lower jaw of each clamp to create a clamping force with the upper jaw that had a steel screw attached. The magnetic clamping force was adjustable to prevent tearing while ensuring no slip, by adjusting the height of the screw and locking it in place with a counter-tightened nut.

Acquisition of force-displacement data

Clots were loaded in between two clamps with fine adjustment enabled by manually operated 3-axis micromanipulators (Cascade Microtech, Beaverton, OR, USA). Each clot began at 6 mm gauge length, and load cells were tared to zero before applying extension. The force recording from the data acquisition software (SensorVUE, Loadstar Sensors, Fremont, CA, USA) and actuation of the nanopositioner were started simultaneously and force measurements were recorded at 30 Hz. The clots were continuously strained to 3 mm at 100 µm/s which was 50% of the initial 6 mm gauge length. Each single experiment was completed within 3 minutes for any given clot including only 30 s for pulls, and replicate clots (typically three) in each set of runs were kept under plastic cover to prevent drying.

Estimation of cross-sectional area of the clot

Prior to applying strain, one digital microscope camera was set to capture top-view images of the clot to extract top cross-sectional dimensions, and a second digital camera was used to capture side-view images to extract thickness. The cameras captured images during the strain loading, each 8 s apart, to obtain true stress from force measurements. The cross-sectional area from the sequence of images were used to convert force measurements to true stress values. ImageJ software (NIH) was used to measure the three top-view images for the width *w* and two side images for thickness *t.* The area of the clot at 10 intervals along the length was calculated by measuring the width and thickness from the top and side view images taken.

S2. Analytical expression for force on prestressed fibrin fibers due to uniaxial tensile strain.

Each fiber element in **Fig. 5B** is assumed to have a linear relationship between axial stress σ and axial strain ε according to Hooke's law $\sigma = E\varepsilon$, where E is the elastic modulus. Letting $\hat{u}$ represent the axial displacement function along the element in the $\hat{e}$ direction, the strain in the element is $\varepsilon = d\hat{u}/d\hat{e}$, where the caret symbol (^) signifies a scalar direction that is always aligned with the longitudinal axis of the considered element. Equilibrium requires that the axial force $F = \sigma A$ be constant along the element, where A is the cross-sectional area of the element. Accordingly, the governing differential equation for the element is as shown in equation S2a.

$$\frac{d}{d\hat{e}}\left(EA\frac{d\hat{u}}{d\hat{e}} \right) = 0 \tag{S2a}$$

Assigning a linear displacement function for $\hat{u}$ and writing in terms of the nodal displacements $\hat{d}_{0x}$ and $\hat{d}_{1x}$ of the end nodes in local coordinates, the displacement function in matrix form is as shown in equation S2b.

$$\hat{u} = \begin{bmatrix} \left(1 - \dfrac{\hat{e}}{L}\right) & \dfrac{\hat{e}}{L} \end{bmatrix} \begin{Bmatrix} \hat{d}_{0x} \\ \hat{d}_{1x} \end{Bmatrix} \tag{S2b}$$

Equation S2c shows the corresponding stiffness equation for the element between node 0 and node 1, in terms of nodal forces $\hat{f}_{0x}$ and $\hat{f}_{1x}$.

$$\begin{Bmatrix} \hat{f}_{0x} \\ \hat{f}_{1x} \end{Bmatrix} = \frac{EA}{L} \begin{bmatrix} 1 & -1 \\ -1 & 1 \end{bmatrix} \begin{Bmatrix} \hat{d}_{0x} \\ \hat{d}_{1x} \end{Bmatrix} \tag{S2c}$$

Similarly, equation S2d shows the notation for a second element between node 1 and node 2.

$$\begin{Bmatrix} \hat{f}_{1x} \\ \hat{f}_{2x} \end{Bmatrix} = \frac{EA}{L} \begin{bmatrix} 1 & -1 \\ -1 & 1 \end{bmatrix} \begin{Bmatrix} \hat{d}_{1x} \\ \hat{d}_{2x} \end{Bmatrix} \tag{S2d}$$

By superposition and using distinct subscripts 1 and 2 for the respective values of area, modulus, and length of each fiber, the global stiffness equation for the two elements in series is shown in equation (S2e).

$$\begin{Bmatrix} F_{0x} \\ F_{1x} \\ F_{2x} \end{Bmatrix} = \begin{bmatrix} k_1 & -k_1 & 0 \\ -k_1 & k_1+k_2 & -k_2 \\ 0 & -k_2 & k_2 \end{bmatrix} \begin{Bmatrix} d_{0x} \\ d_{1x} \\ d_{2x} \end{Bmatrix} \tag{S2e}$$

By symmetry of placing node 0 at the origin of the quadrant, $d_{0x} = 0$. For tensometric loading, the end displacement d_{2x} is a prescribed value δ. There is no externally applied force at node 1, such that $F_{1x} = 0$. With these boundary conditions, the solution reduces to two equations and two unknown (S2f).

$$\begin{Bmatrix} 0 \\ F_{2x} \end{Bmatrix} = \begin{bmatrix} k_1+k_2 & -k_2 \\ -k_2 & k_2 \end{bmatrix} \begin{Bmatrix} d_{1x} \\ \delta \end{Bmatrix} \tag{S2f}$$

The solution to the scenario with only a prescribed external displacement is straightforward with $d_{1x} = k_2\delta/(k_1+k_2)$ and the axial force $F_{2x} = F$ as shown in equation (S2g).

$$F = \left(k_2 - \frac{k_2^2}{k_1+k_2} \right) \delta \tag{S2g}$$

The strain energy in each specific element i can be computed from stored elastic energy $\frac{1}{2}k_i u_i^2$ nodal displacements, where the axial displacement u_i is computed from the difference in nodal displacements (e.g., $u_1 = d_{1x} - d_{0x}$). The corresponding strain energy density for each element or for the overall system is computed by dividing by respective volume.

We make two important modifications to the basic two-element solution above for our pre-strained discrete fiber model. First, at node 1 (i.e., location of the focal adhesion) we add a contractile force $F = -\alpha EA$, for which the elastic modulus E and cross-sectional area A pertain to the platelet aggregate. Entering this force into the global stiffness equation and simplifying reduces the system to two equations (S2h).

$$\begin{Bmatrix} -\alpha EA \\ F_{2x} \end{Bmatrix} = \begin{bmatrix} k_1+k_2 & -k_2 \\ -k_2 & k_2 \end{bmatrix} \begin{Bmatrix} d_{1x} \\ \delta \end{Bmatrix} \tag{S2h}$$

The extent of aggregate compaction from an initial radius R_0 to a compacted radius R_c can be described either by the compaction strain α or alternatively in terms of compaction ratio $\zeta = R_0/R_c = 1/(1-\alpha)$. With compaction, the displacement at node 1 becomes $d_{1x} = (k_2\delta - \alpha EA)/(k_1 + k_2)$. Equation (S2i) shows the modified solution for axial force when prestrain is taken into account.

$$F = \left(k_2 - \frac{k_2^2}{k_1+k_2} \right) \delta + \frac{k_2 EA}{k_1+k_2} \alpha \tag{S2i}$$

Second, we account for multi-directional orientation of fibers using coordinate transformations for fibers that are oriented off-axis from the direction of externally applied strain. Coordinate transformation is achieved by using a rotation matrix to allow any

element oriented at an angle θ (measured counter clockwise from the global x-axis) to be mapped to global displacements d_x and d_y as shown in equation S2j.

$$\begin{Bmatrix} \hat{d}_x \\ \hat{d}_y \end{Bmatrix} = \begin{bmatrix} \cos(\theta) & \sin(\theta) \\ -\sin(\theta) & \cos(\theta) \end{bmatrix} \begin{Bmatrix} d_x \\ d_y \end{Bmatrix} \tag{S2j}$$

This prestress model formulation was verified using finite element analysis (FEA) by taking advantage of the "thermal force" analogy used to model thermal expansion and contraction. The FEA computational solutions matched analytical solutions exactly for the entire range of relative size, relative modulus, compaction ratio, and orientation angles.

S3. Supplementary Figures

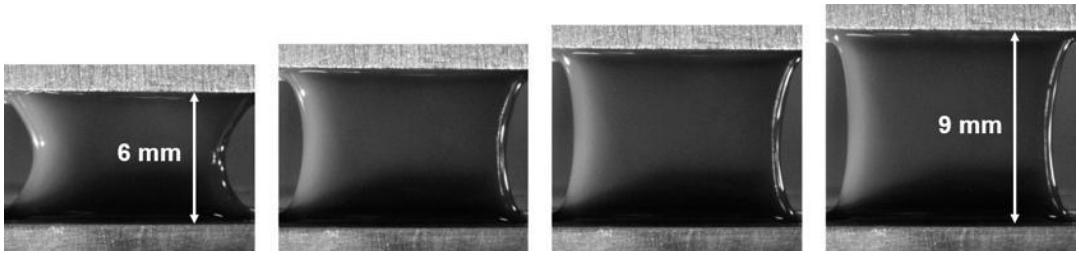

Figure S1. Real time images of clots as the clots are pulled by microtensometer to a maximum of 50% strain

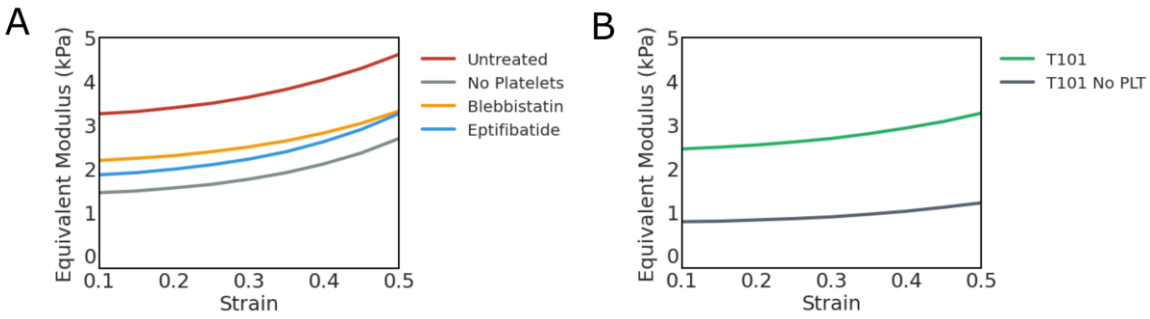

Figure S2. Equivalent modulus of the clots evaluated from the nonlinear exponential model at indicated strains.

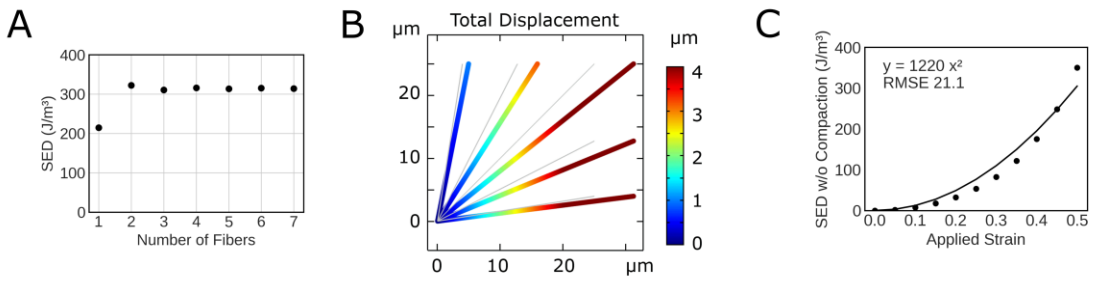

Figure S3. Characterization of discrete prestressed fiber model. (A) Convergence plot for strain energy density at 50% tensile strain and constant modulus (4.4 kPa), computed from a discrete fiber model consisting of different numbers of fibers; (B) Deformation of a prestressed fiber model of clot at 25% tensile strain without any platelet contraction (i.e., fibrin fibers only); (C) Strain energy density at 50% applied strain in the absence of any contractile strain shows approximately quadratic increase with externally applied strain, where RMSE = root mean square error.

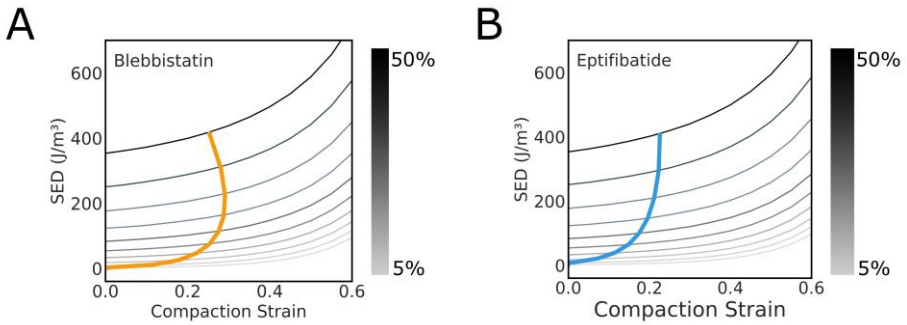

Figure S4. Mapping of experimental strain energy densities at applied strains from 5% to 50% onto predictions from discrete prestressed fiber model for blebbistatin (A) and eptifibatide (B) treatments.